

Three-dimensional P velocity structures of the lithosphere beneath Taiwan from the analysis of TAIGER and related seismic data sets

Hao Kuo-Chen,¹ Francis T. Wu,¹ and Steven W. Roecker²

Received 18 December 2011; revised 25 April 2012; accepted 29 April 2012; published 7 June 2012.

[1] The convergence of the Philippine Sea and the Eurasian plates in the Taiwan region led to the formation of a young collisional mountain between two subduction zones of nearly orthogonal polarities. The geological processes underlying the collision and its relation to subduction are the primary targets of TAIGER (Taiwan Integrated Geodynamic Research) project. Newly acquired passive and active sources data on land, supplemented by ocean bottom as well as permanent seismic network data, are used to derive a new 3-D tomographic velocity model. Using the 7.5 km/sec contour as a marker for crustal deformation, two trend-parallel “roots,” one under the Central Range with a maximum depth of 55 km and the other under the Coastal Range at 40 km, are found to extend from southern to central ($\sim 24^\circ\text{N}$) Taiwan. Between the two roots and lying approximately beneath the Longitudinal Valley, the 7.5 km/sec contour rises to 25 km depth. In the upper mantle, a high velocity zone, east-dipping and its upper surface coinciding with a Wadati-Benioff zone in the south ($\sim 22.8^\circ\text{N}$), becomes near vertical and ill-defined in the north ($\sim 23.9^\circ\text{N}$). The crustal deformation as defined by the “roots” and the along-trend variations of the upper mantle structures under Taiwan provide key information for the orogeny. With the thickening of crust to 55 km or more processes such as eclogitization and delamination may come into play.

Citation: Kuo-Chen, H., F. T. Wu, and S. W. Roecker (2012), Three-dimensional P velocity structures of the lithosphere beneath Taiwan from the analysis of TAIGER and related seismic data sets, *J. Geophys. Res.*, 117, B06306, doi:10.1029/2011JB009108.

1. Introduction

[2] The young (~ 6.5 Ma) and active Taiwan orogen is known to be a result of an oblique collision between the Philippine Sea plate (PSP) and the Eurasian plate (EUR) [Big, 1981; Chai, 1972]. Currently, as defined by seismicity and available velocity images, the Philippine Sea plate subducts northwestward under the Eurasian plate along the Ryukyu Trench in northern Taiwan (Figure 1) while the Eurasian plate subducts eastward under the Philippine Sea plate both in southern Taiwan and along the Manila Trench farther to the south [e.g., Wu *et al.*, 1997]. In the main collision zone, the principal geologic/tectonic units at the surface (Figure 1) are defined from east to west as follows: (1) the Coastal Range (CoR), the compressed Luzon Arc and its forearc; (2) the Longitudinal Valley Fault (LVF), the suture between the Eurasian and Philippine Sea plates that separates the CoR from (3) the pre-Tertiary basement of the continental margin of the Eastern Central Range (ECR), known as the

Tananao Complex (TC); (4) the Backbone Range (BR), composed of Miocene to Eocene slates; (5) the Hsuehshan Range (HR), built mostly from Eocene and Oligocene continental shelf sediments from the west; (6) the Western Foothills (WF), composed of accreted and deformed sediments in the foreland basin; and (7) the Coastal Plain (CP), the present-day foreland basin [Ho, 1986].

[3] The tectonics of the orogen itself is far from clear, and a variety of conceptual models have been proposed. As examples: (1) a thin-skinned crust shortened over a shallow detachment [Suppe, 1981]; (2) deformation of the lithosphere to form the Taiwan orogen [Wu *et al.*, 1997]; (3) continental subduction of the Eurasian plate with crustal exhumation [Lin, 2002]; or (4) flipping or breaking of the subducting Eurasian plate [Teng *et al.*, 2000; Lallemand *et al.*, 2001]. One can pose diagnostic questions for each of these scenarios checking them against empirical observations. For example, are the orogenic processes restricted to the shallow crust?, is there a throughgoing detachment across Taiwan?, does orogenic deformation occur throughout the whole crust?, what are the accompany processes in the upper mantle?, and does the Eurasian plate subduct actively beneath central and northern Taiwan as an aseismic subduction zone and, if so, how does it occur?. These questions can be at least partially addressed by more detailed subsurface velocity images down to upper mantle depths.

[4] Seismic imaging in general, and arrival time tomography in particular, can provide critical evidence related to these questions, and indeed this has motivated a number of

¹Department of Geological Sciences and Environmental Studies, State University of New York at Binghamton, Binghamton, New York, USA.

²Department of Earth and Environmental Sciences, Rensselaer Polytechnic Institute, Troy, New York, USA.

Corresponding author: H. Kuo-Chen, Department of Geological Sciences and Environmental studies, State University of New York at Binghamton, Binghamton, NY 13902, USA. (kuochen.hao@gmail.com)

Copyright 2012 by the American Geophysical Union.
0148-0227/12/2011JB009108

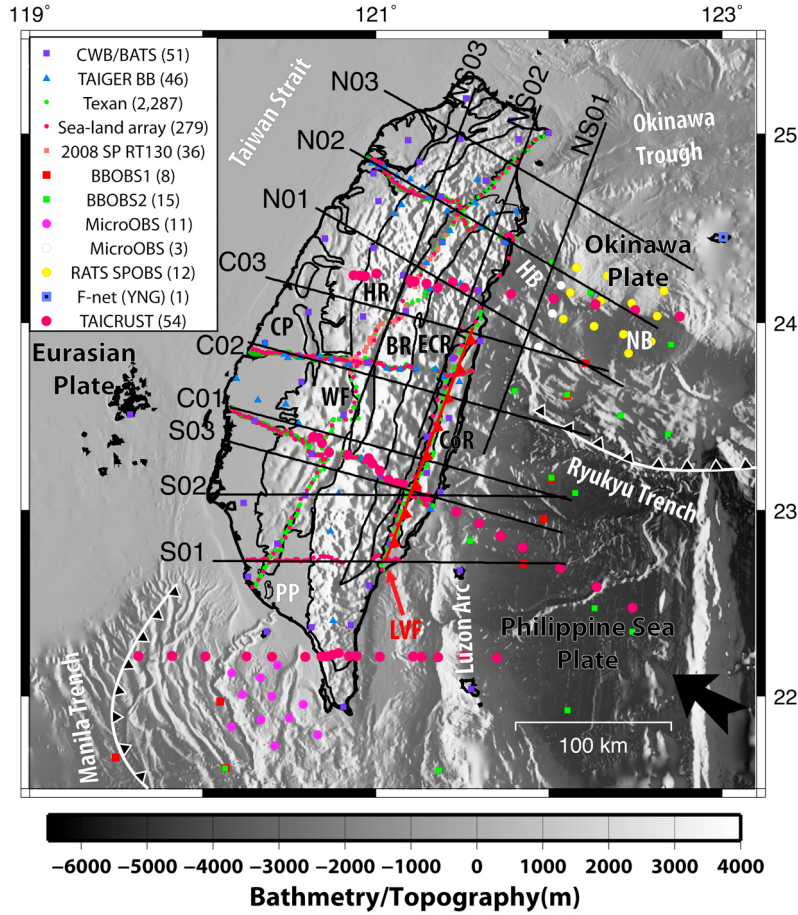


Figure 1. Tectonic setting of Taiwan and seismic stations used in this study. Black arrow: the relative plate motion (82 mm/yr [Yu *et al.*, 1997]). CP: Coastal Plain. WF: Western Foothills. HR: Hsuehshan Range. BR: Backbone Range. ECR: Eastern Central Range. CoR: Coastal Range. LVF: Longitudinal Valley Fault. PP: Pingtung Plain. HB: Hoping Basin. NB: Nanao Basin. Manila and Ryukyu Trenches are drawn on the basis of bathymetry only. Black segments: locations of cross-sections in Figures 8–12.

previous tomographic investigations of the crust and upper mantle of Taiwan. Since the seminal study of Roecker *et al.* [1987], several investigators [e.g., Rau and Wu, 1995; Ma *et al.*, 1996; Kim *et al.*, 2005; Wang *et al.*, 2006; Y.-M. Wu *et al.*, 2007] have generated 3D arrival-time tomography images of Taiwan using progressively larger data sets and improved techniques. All of these studies analyzed primarily short-period seismic phase data collected from networks operated by the Institute of Earth Science (IES) and the Central Weather Bureau (CWB). In several respects, these data were less than ideal; station coverage of the early IES network was sparse, and timing of the short period CWB data reportedly has uncertainties of up to a few tenths of a second [Chou *et al.*, 2009; Chang *et al.*, 2012]. In addition, most of these studies used recordings only of local earthquakes, which means that subcrustal features are poorly sampled. Generally, the upper mantle can be imaged with local events only under northern Taiwan where the Ryukyu subduction events are plentiful and station coverage is dense. Wang *et al.* [2006, 2009] used a combination of local earthquakes and teleseisms recorded on Taiwan and a few stations on the SE coast of China to resolve a high velocity zone underneath southern and northern Taiwan at least as far as 24°N.

However, as discussed below, parts of their models appear to contradict other models and thus raise further questions to be answered. Using an alternate approach, Lallemand *et al.* [2001] and Bos *et al.* [2003] reinterpreted the global tomography models of Bijwaard *et al.* [1998], which are based on teleseismic arrivals recorded by global networks and published by International Seismological Center (ISC) and the National Earthquake Information Center (NEIC). While the resolution of structure within the crust and uppermost mantle from the ISC and NEIC data is less than that from local data, their analysis suggests that the slab of the Eurasian plate subducts to the east beneath most of Taiwan to depths as great as 670 km.

[5] Uneven station density and a limited aperture of the local land-based seismic networks hampered the tomographic inversion using existing data. The resulting lack of sampling, especially in the shallow crust, and crossing rays in the mantle mean that key structures beneath the Taiwan orogen remain poorly illuminated. For this reason, one of the main objectives of Taiwan Integrated Geodynamic Research (TAIGER) project was to improve the tomographic images of the crust and upper mantle by densifying the land seismic networks and deploying ocean-bottom seismographs offshore

of Taiwan. Several active source profiles were carried out as part of TAIGER as well, and, in addition to recording shots, these stations operated continuously and thereby recorded a large number of local earthquakes and a couple of teleseisms. In this paper, we describe the results of an arrival time tomography of a data set formed from the TAIGER active and passive seismic data and augmented with readings from existing broadband networks. The extended aperture and significantly greater density of both events and stations provides significantly better resolved images than previous studies.

2. Data

[6] Data from the combined TAIGER and permanent broadband networks on and around Taiwan are used and the networks and their locations are shown in Figure 1. Among the TAIGER deployments on land, the broad band and the short period (2 Hz) onshore/offshore stations along four transects are GPS-equipped, and the short period Texans (4.5 Hz), closely spaced recorders deployed along three transects are synchronized before and after a duration of up to five days; furthermore, there were also more coarsely spaced NS lines of stations (Figure 1). Although primarily intended for recording the active sources, the TAIGER short period stations recorded continuously, thus allowing recording of earthquakes as well. Previous tomographic investigations of Taiwan used phase data from a large number of local earthquakes, typically in excess of 10,000 [e.g., *Kim et al.*, 2005; *Y.-M. Wu et al.*, 2007]. However, because the station spacing is on the order of a few tens of kilometers, the shallow part of the crust is usually not well sampled. In the TAIGER data set, fewer earthquakes were available due to the shorter duration of deployments but because we use a larger number of stations, with separations at 200 m for active source arrays and 2 km for offshore/onshore arrays, we can balance the number of stations with the number of earthquakes, gaining better resolution of laterally varying features with increased areal ray coverage.

[7] The TAIGER land-based broadband stations were deployed not only along three main transects, but also in the mountainous areas in northeast Taiwan where existing stations of the permanent BATS (Broadband Array in Taiwan for Seismology) and CWB broadband networks are sparse (Figure 1). The TAIGER ocean-bottom broadband seismometer deployments widened the existing areal coverage east of Taiwan; however, shallow water depth and fishing activities prevented a similar deployment in the Taiwan Strait. Finally, to further extend coverage offshore, we added readings from (1) station YNG of the NIED, Japan, network, (2) a short period OBS network operated as part of the French RATS (Ryukyu Arc: Tectonics and Seismology) network [*Theunissen et al.*, 2012], (3) a short period OBS network deployed for a week southwest of Taiwan [*Liao et al.*, 2008], and (4) short period air gun arrivals from the TAICRUST (a joint Taiwan-United States geophysical project) investigation [*McIntosh et al.*, 2005]. We note that inclusion of the RATS and TAICRUST data significantly increases the tomographic resolution of the offshore regions. In total, data from 2,803 stations are used in this study. To assess the robustness of our models, based on the TAIGER arrival times, we derived a model using the same tomography code

but with phase data from the short period island-wide CWB digital seismic network (TAISN) that has been in operation since 1991; previous tomographies of Taiwan cited earlier [*Rau and Wu*, 1995; *Kim et al.*, 2005; *Y.-M. Wu et al.*, 2007] used similar data set.

[8] Except for data from TAISN and TAICRUST, for which phase picks were generated by previous investigators, we used the AIC picker [*Maeda*, 1985] for automatic P phase picking of arrivals from explosions and local earthquakes. The time window of the AIC picker is 5 s before and after an estimated P arrival time based on a 1-D layer model for the Taiwan region [*Shin and Chen*, 1988] and the CWB catalog location. The auto-picking results are visually reviewed and adjusted as necessary. Cross-correlation was used to pick teleseismic P arrival times and only events with more than 5 stations recording P waves that are well correlated (normalized cross-correlation coefficient >0.7) are selected. The total data set consists of 10 TAIGER shots with ~6,000 readings, 3,011 local events with ~53,000 readings, 568 teleseismic events (distance of 30°–90°) of magnitude $M_b > 5.5$ with ~11,000 readings (Figure 2), and 14,175 air gun readings from the TAICRUST.

3. Methodology

[9] We analyze the P-picks using the finite difference arrival time tomography algorithm described in *Roecker et al.* [2004, 2006] to obtain 3D velocity structures. Because our region of interest (~600 × 600 km) is too large to be treated accurately as a flat Earth, and also to avoid the biases introduced by either inserting a spherical Earth in a Cartesian system or applying Earth flattening transforms to a laterally heterogeneous model, we compute travel times by adapting an eikonal equation solver based on that of *Vidale* [1988] and *Hole and Zelt* [1995] directly to a spherical coordinate system. Specifically, the eikonal equation solved is

$$\left(\frac{\partial t}{\partial r}\right)^2 + \left(\frac{1}{r} \frac{\partial t}{\partial \theta}\right)^2 + \left(\frac{1}{r \sin \theta} \frac{\partial t}{\partial \phi}\right)^2 = s^2$$

where t is travel time, s is slowness, θ and ϕ are geocentric colatitude and longitude, respectively, and r is the distance of the center from the earth.

[10] The arrival time tomographic inversion involves two principal steps. The first locates local earthquakes in a starting model through an interpolated grid search. The second calculates raypaths from all sources to recording stations and forms a system of linear equations that are then solved for perturbations to P-velocities. While the hypocenters of local earthquakes are relocated in each iteration, shot and teleseismic locations are held fixed, with teleseismic raypaths within the model determined using Fermat's principle.

3.1. “Regional” and “Local” Tomographic Inversions

[11] The tomographic computations were done on a quad CPU, dual-core desktop computer. Several steps were taken to enable each run to finish within a few days. For example, storing the travel-time tables for each station speeds up event relocation significantly. The unusually large number of stations (2803) used in our analysis and the large 3D volume that we are attempting to image could generate significant computational load. Our strategy for extracting as much

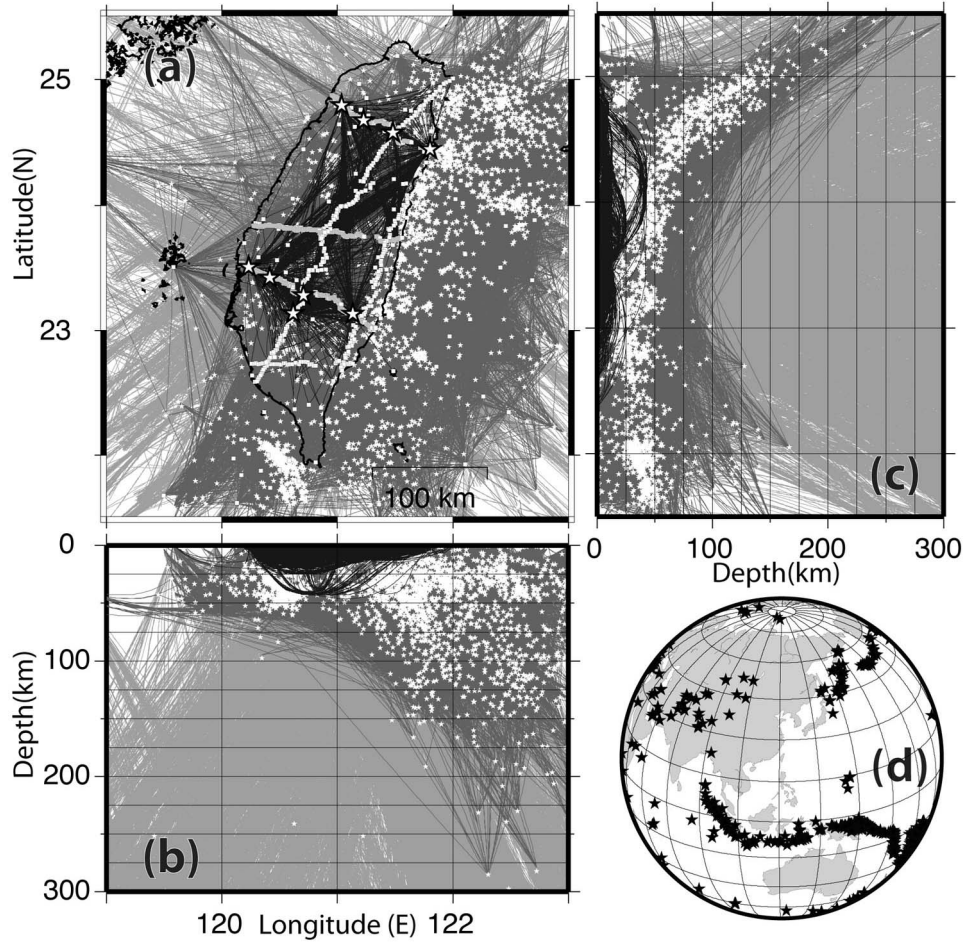


Figure 2. Raypaths with different source locations. (a) Map view of raypath coverage, source locations and station locations. Raypaths are shown as lines: Black-explosion; Darker gray-local earthquake; Lighter gray-distant earthquake. Sources: Small white star-local earthquake; Big white star-explosion; White square-seismic station. (b) East-west cross-section with raypaths. (c) North-south cross-section with raypaths. (d) Locations of teleseisms (black stars) in orthographic projection with Taiwan at the center and 90° to the edge.

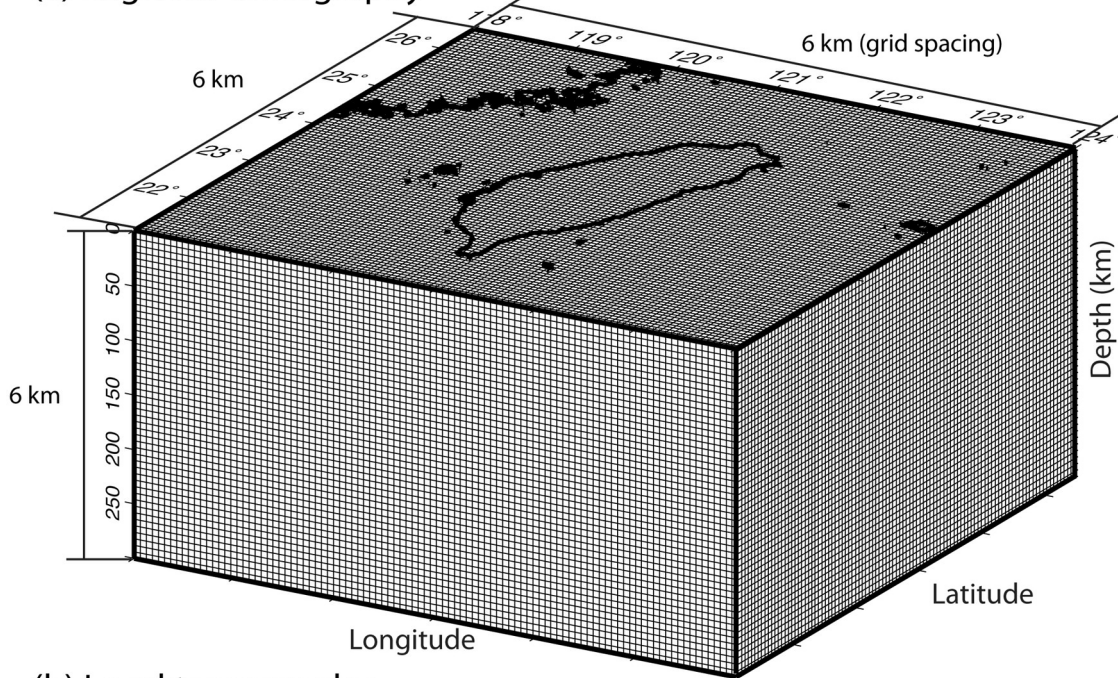
useful information as possible from the data while maintaining tractability is to generate models with two grid systems: one “local” system with a fine grid spacing that focuses on near-surface structure, and a coarser “regional” grid system that extends from the surface to 300 km depth. The logic for this choice is straightforward: the number of raypaths and level of heterogeneity are greater in the local system while the depth of penetration is less, so a finer spacing is both warranted and tractable. The coarser spacing allows us to analyze the total data set and extend the model to greater depths, where ray coverage is less dense but heterogeneity is also likely less pronounced. As discussed below, this mode of analysis has the side benefit of providing an additional test of robustness since it allows us to assess the influence of grid spacing on the resulting image. In particular, one would expect that the image from the coarser, regional model should look like a smoothed version of that obtained from the finer, local model. For the regional scale tomography (Figure 3a), we tested a series of grid sizes and found that a $6 \times 6 \times 6$ km 3 equally spaced grid allows for adequate spatial resolution for crustal and mantle features of dimensions \sim 6 to 60 km or

larger (note that the frequency band of teleseismic events around $1 \sim 0.1$ Hz). Coarser grids rendered overly smooth anomalies and finer grids tended to generate oscillating high and low velocity anomalies in the mantle, a symptom of unresolved tradeoffs. The model we use is 600 km long in both horizontal directions and 300 km in depth. In each case, the starting model is the 1D model determined by *Shin and Chen [1988]* for the Taiwan region. For local tomography, we included only the arrival times from local sources (i.e., no teleseisms). We use non-uniform grids in order to allow finer resolution where station density is relatively high. From the center to the edge of the model, the grid intervals vary laterally from 4 km to 16 km. In the vertical direction the grid intervals vary from 2 km in the top 24 km, 4 km from 24 to 64 km depth, 8 km from 64 to 96 km depth and then 10 km at 116 km (Figure 3b).

4. Results

[12] After 8 iterations, the final 3D regional model (hereafter referred to as the pf3DRegional model) the data variance

(a) Regional tomography



(b) Local tomography

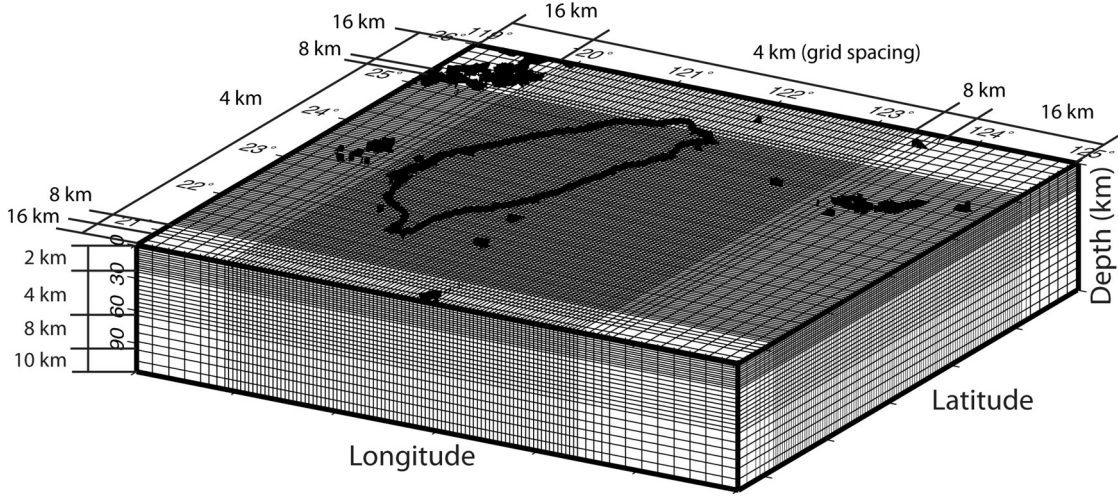


Figure 3. The discretization of the regional and local tomographic models. (a) The dimension of the model for regional tomography is $EW \times NS \times Z = 600 \times 600 \times 300 \text{ km}^3$ and the grids are $6 \times 6 \times 6 \text{ km}^3$. (b) The total dimension of the local tomography is nearly the same in the horizontal directions but only extends to 116 km depth. The grid spacing is variable. In the main area of interest, the grid spacing is 4 km in the east-west and north-south and changes to 8 and then 16 km spacing toward the edges of the model. In the vertical direction, the grid intervals are 2 km in the top 24 km, 4 km from 24 to 64 km, 8 km from 64 to 96 km and then at 10 km from 96 km to 116 km.

reduced from 0.3128 s^2 to 0.0995 s^2 ($\sim 68\%$) (Figures 4 and 5). The final local tomography model, pf3D_local, was achieved after 5 iterations and the data variance reduced from 0.8279 s^2 to 0.2056 s^2 ($\sim 75\%$). In both cases, the iteration continued until the reduction in data variance was insignificant.

[13] Viewed in horizontal cross section, the shallow structures in the pf3DRegional velocity model (Figures 6a and 6b) correspond quite well with major geologic units

(Figure 1). The mountains of the Hsuehshan, Backbone, and Eastern Central Ranges are underlain by high velocity ($V_p > 5 \text{ km/sec}$ and $dV_p > 0$) rocks, with the highest ($dV_p > 10\%$) appearing in northeast part of the Eastern Central Range, where the pre-Tertiary metamorphic rocks of the Tananao Complex are exposed at the surface. In contrast, the Coastal Plain on the west and the Coastal Range on the east are underlain by low velocity ($V_p \sim 4 \text{ km/sec}$ and $dV_p < 0$) rocks (Figure 6), with the lowest negative dV_p

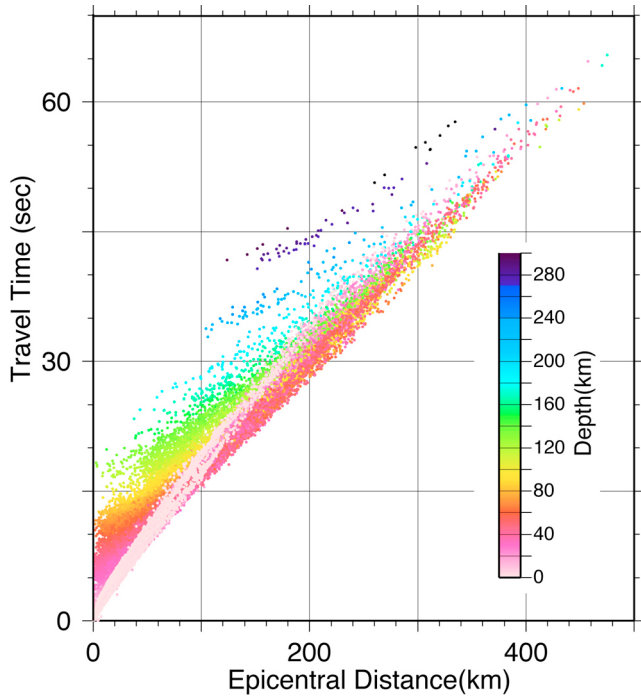


Figure 4. Travel time versus epicentral distance for explosions and local earthquakes. The local earthquakes were relocated in the pf3D_{regional} tomography.

(<10%) occurring beneath the Pingtung Plain in southwestern Taiwan (Figures 1 and 6). The low velocities beneath the Coastal Range are due to the forearc basin and the remnant Luzon arc. The dVp = 0% ($V_p = 4.76 \text{ km/sec}$) contour that separates the high from the low velocity regions coincides closely to the boundaries between the high ranges and Western Foothills (Figures 1 and 6).

[14] Similar patterns occur at a depth of 6 km (Figure 7), although the Hoping and Nanao Basins appear as relative low velocity zones, and a higher velocity anomaly begins to

emerge east of the Penghu Island (Figures 7a and 7c). This Penghu high is connected to the “Peikang basement high” of western Taiwan at greater depth (Figures 7b and 7c). At 12 km depth, the velocity patterns begin to reverse: a relatively low velocity zone appears beneath the Backbone Range area and a relatively high velocity zone beneath the southern Coastal Range. The PSP area offshore of eastern Taiwan has mostly high velocities between 6 and 42 km depth (Figures 7a and 7e).

[15] The dVp patterns between the depths of 18 to 54 km are the opposite of those at shallow depths (especially those between 0 to 6 km), with relatively high velocities beneath the Coastal Plain, the Western Foothills, and the Coastal Range areas and low velocities beneath the Hsuehshan Range, the Backbone Range, and the Eastern Central Range. At a depth of 18 km, a large positive dVp (>10%) appears to the east of the Coastal Range and extends throughout most of the Coastal Range. Between 18 and 42 km depth, a large positive dVp (>10%) zone under the Coastal Range extends seaward. However, dVp beneath the Central Range is negative (dVp = 0 to -5%) between 18 and 54 km depth (Figures 7c and 7f), indicating the presence of the low velocity root under the Central Range. This change in sign in dVp is similar to that found in several previous tomographic investigations [Roecker et al., 1987; Rau and Wu, 1995; Kim et al., 2005; Y.-M. Wu et al., 2007].

[16] Patterns at greater depths (84–150 km) are simpler than those at shallow depths. A positive dVp appears beneath central Taiwan at a depth of 84 km and extends under southern as well as northern Taiwan. This positive dVp zone, however, appears to shift eastward as it goes deeper (Figure 7h).

[17] Several of the features described above are easier to track in vertical cross-sections. Above 60 km depth, the vertical cross-sections taken from the pf3d_{regional} and the pf3d_{local} models; the cross sections are presented in left and right panels, respectively, in Figures 8–11) are generally similar to each other. However, as may be expected, many fine structures in the crust are discernible only in pf3D_{local}.

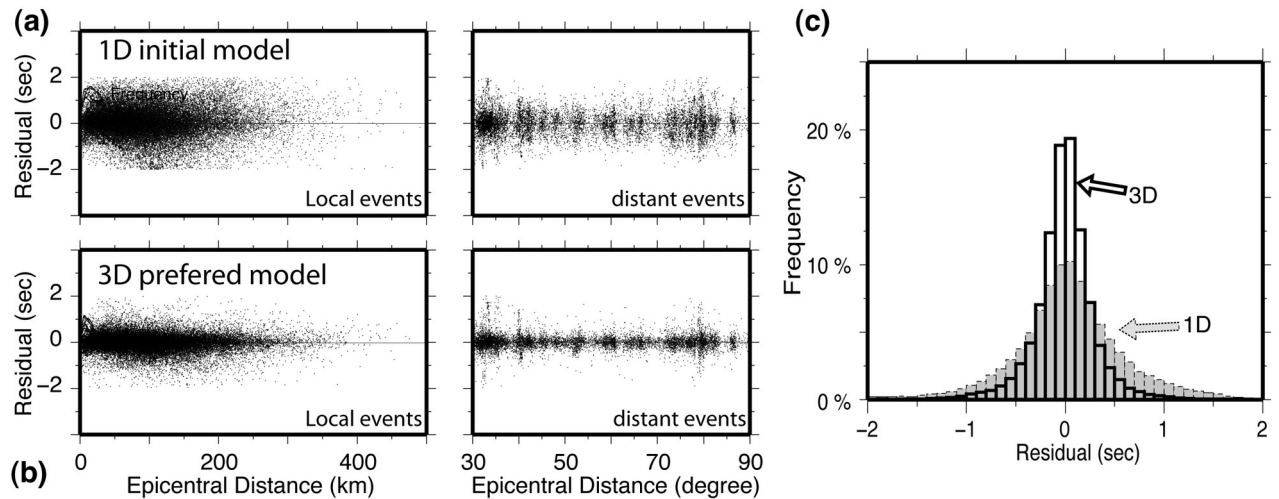


Figure 5. Travel time residuals from the 1D (initial) and the pf3D_{regional} velocity models. (a) Travel time residuals from the 1D model; (b) travel time residuals from the pf3D_{regional}; (c) travel time residuals comparisons between the 1D initial model and the pf3D_{regional}.

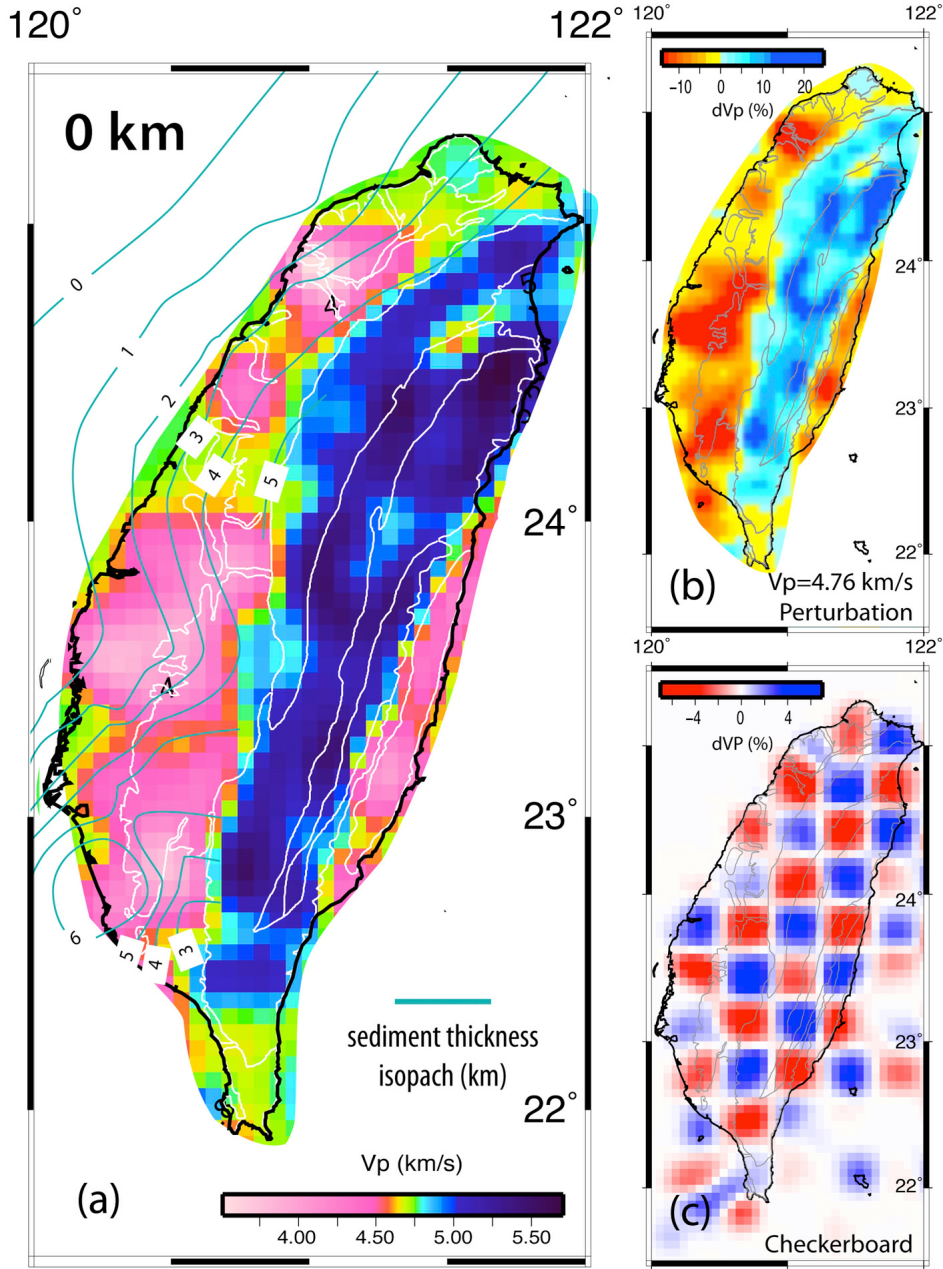


Figure 6. The pf3DRegional slices at a depth of 0 km. (a) Absolute velocity model with depth to basement from Lin and Watts [2002]; (b) dV_p from the 1D initial model; (c) checkerboard test result.

In the discussion below, we focus our attention on the local model when discussing features above 60 km and primarily on the regional model when referring to upper mantle structures.

[18] Of particular interest is the change in crustal structures across the orogen. The integrative nature of arrival time tomography does not allow the precise identification of an interface like the Moho. In Taiwan, several investigations [Ma and Song, 1997; Chen et al., 2003; Liang et al., 2007] aimed at the derivation of Moho velocity and they estimated a Pn-velocity of 7.8–8.0 km/sec using mainly earthquake data. The rapidly varying velocity structures across Taiwan however render the direct measurement of Pn difficult. In this paper, we have chosen the 7.5 km/sec velocity contour as a

marker to trace the change in the variations of the crust. Cross sections (Figures 8–10, profiles S01–N01) show that the maximum depth of the 7.5 km/sec contour increases gradually from south to central Taiwan and then decreases dramatically in the north (section N03 in Figure 10). A persistent feature (Profiles S01–N01 in Figures 8–10) is a downwarping of the 7.5 km/sec contour that nearly mirrors the topography. A “transition layer” confined between the 7.5 and 8 km/sec contours follows the 7.5 km/sec contour without much change in thickness beneath western Taiwan and the Central Range, but thickens toward the east starting from the deepest point of the 7.5 km/sec contour (Profiles S02, S03, C01–C03 and N01 of Figures 8–10). A smaller, shallower “root” beneath the area east of the Coastal Range can

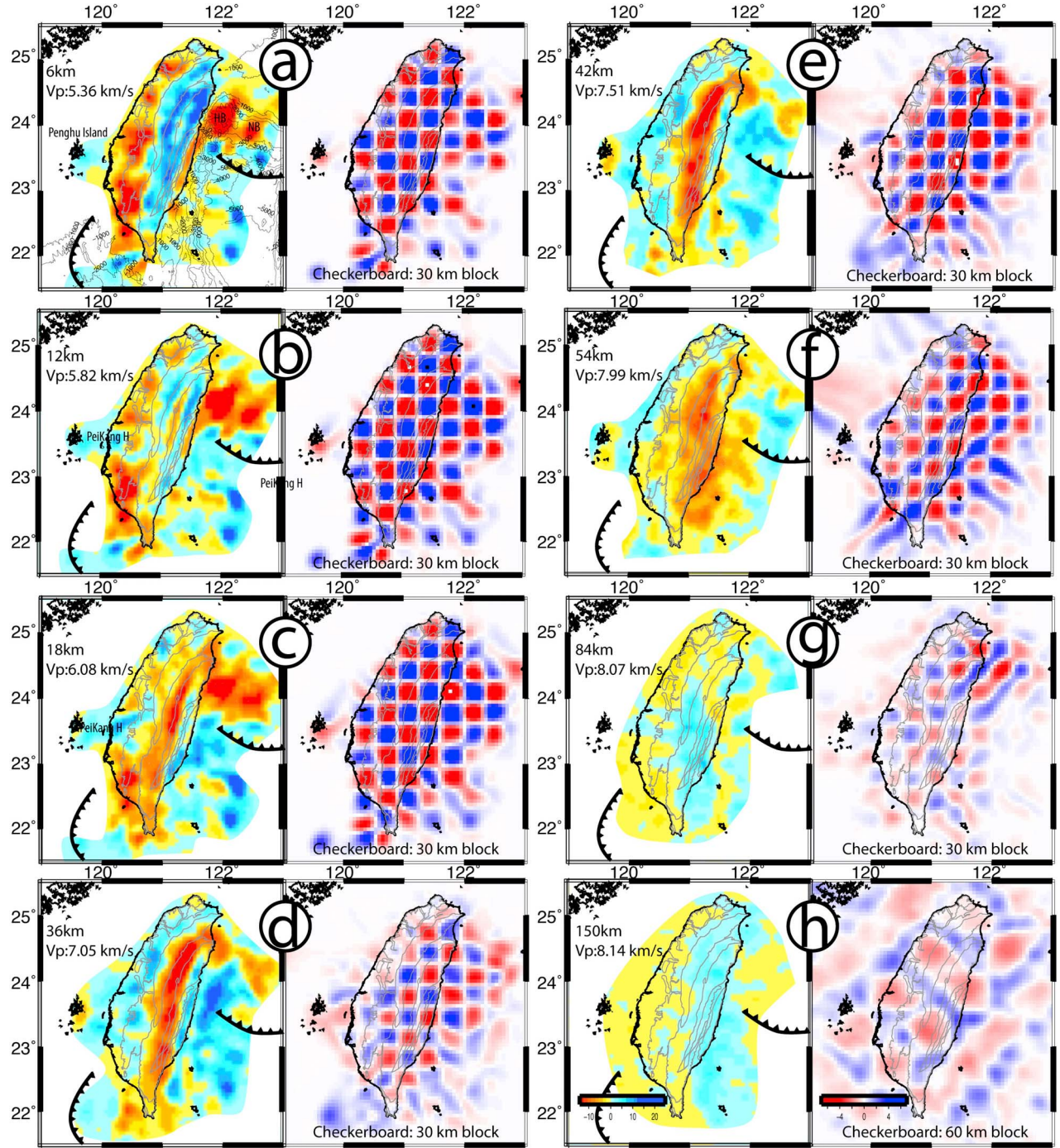


Figure 7. (a–h) Relative velocities (dV_p) at different depths with the associated checkerboard test results from the pf3D_{_}regional model.

also be seen (Profile S02, S03, and C01-C03 in Figures 8 and 9). The well-defined east dipping seismic zone plotted in profiles S02, S03 and C01 (Figures 8 and 9) just above the smaller root was recognized as the plate boundary between the PSP and the EUR after a Mw6.8 earthquake in 2003 [e.g., Kuo-chen et al., 2007]; this seismic zone projects to the LVF at the surface. Between the two “roots” the 7.5–8.0 km/sec zone thickens and the 7.5 km/sec contour rises, (e.g., Profile C03; Figure 9) from >60 km to <30 km; the variations of this

feature can be found in profiles from S01 to C03 (Figures 8 and 9). Beneath the Coastal Plain and the Western Foothills, a low velocity layer exists between 0 and 10 km depths; it corresponds to the sedimentary basin of western Taiwan (Figures 8–10, local and regional).

[19] Velocity structures of the Central Range are complex. The Central Range is underlain by relatively high velocities at shallow depth as mentioned above (e.g., in profile C02 of Figure 9 and also Figures 7a and 7b); the 5.5–6 km/sec

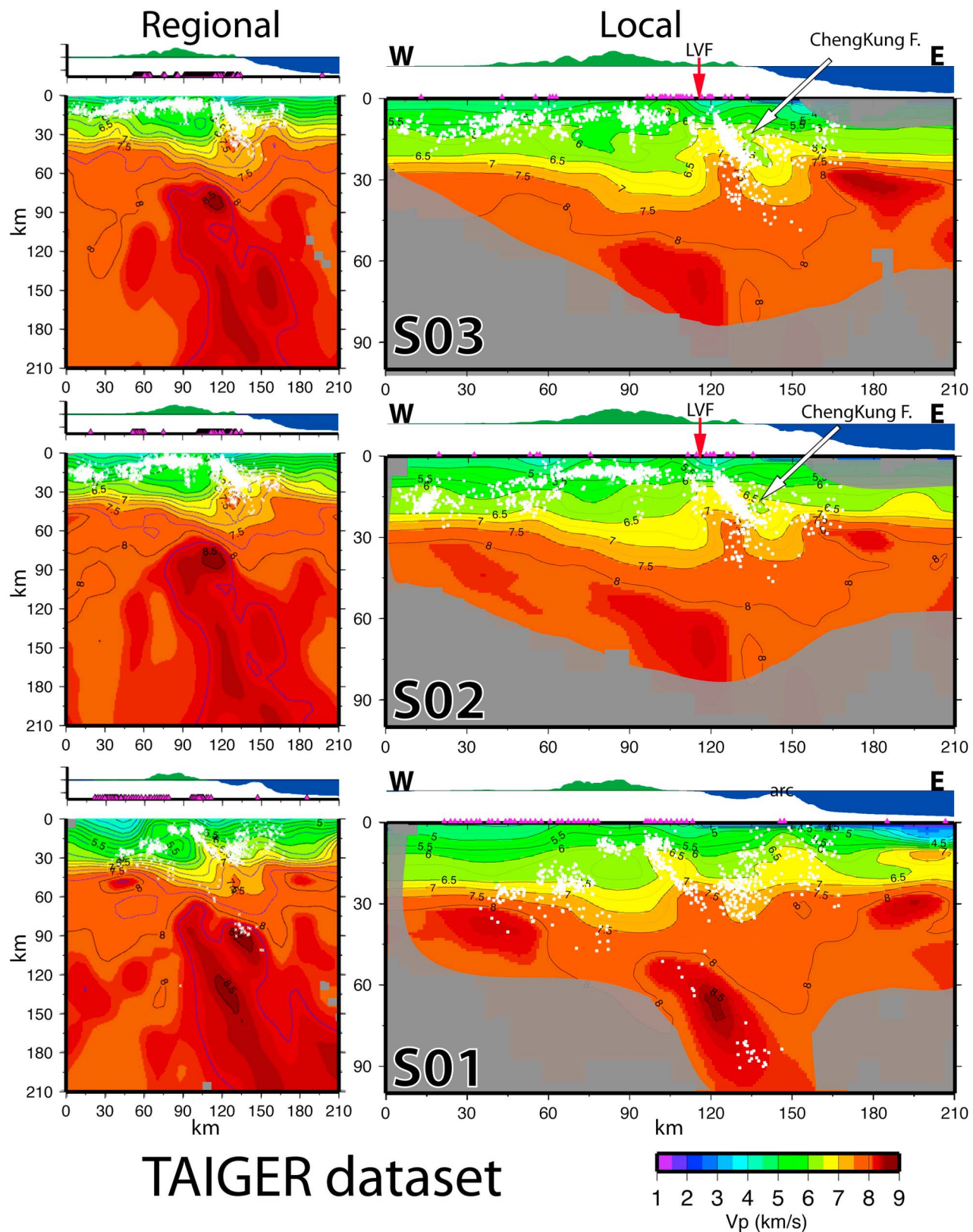


Figure 8. East-west tomographic sections of absolute velocity in southern Taiwan. The locations of the sections are shown in Figure 1. (left) From the regional model (pf3D_{regional}). (right) From the local model (pf3D_{local}). White dots: earthquakes.

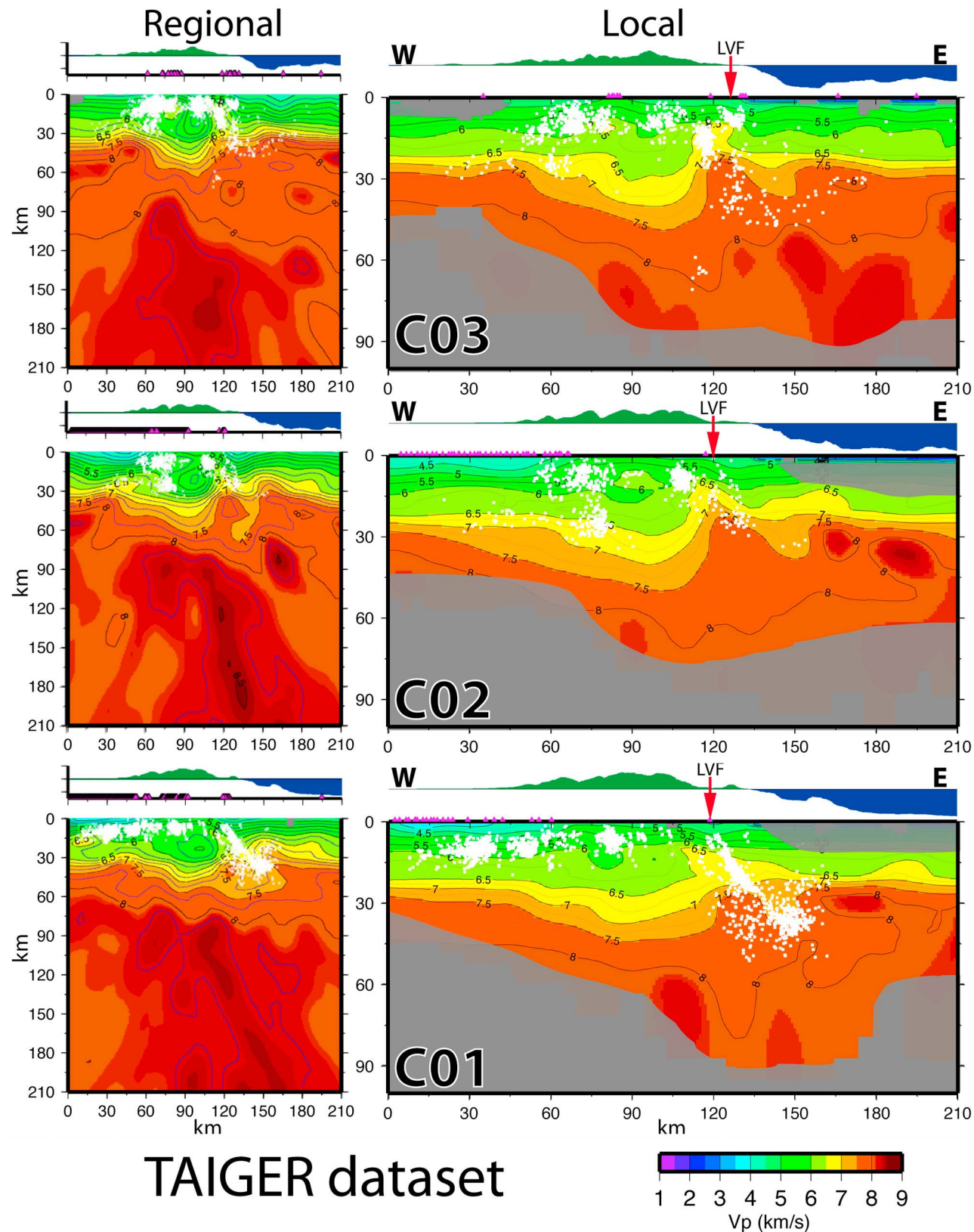


Figure 9. East-west tomographic sections of absolute velocity in central Taiwan. The locations of the sections are shown in Figure 1. (Left) From the regional model (pf3DRegional). (right) From the local model (pf3DLocal). White dots: earthquakes.

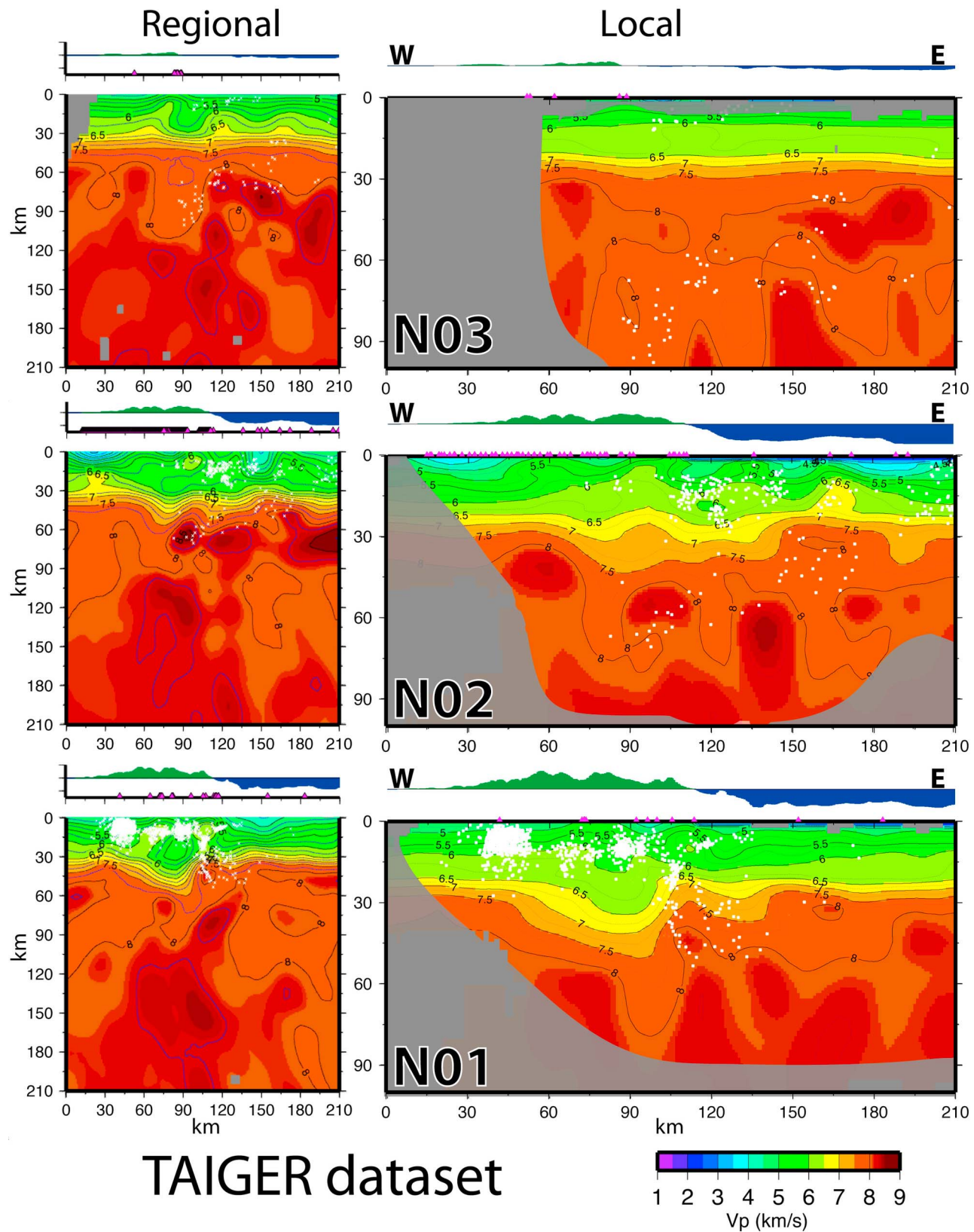


Figure 10. East-west tomographic sections of absolute velocity in northern Taiwan. The locations of the sections are shown in Figure 1. (left) From the regional model (pf3D_{regional}). (right) From the local model (pf3D_{local}). White dots: earthquakes.

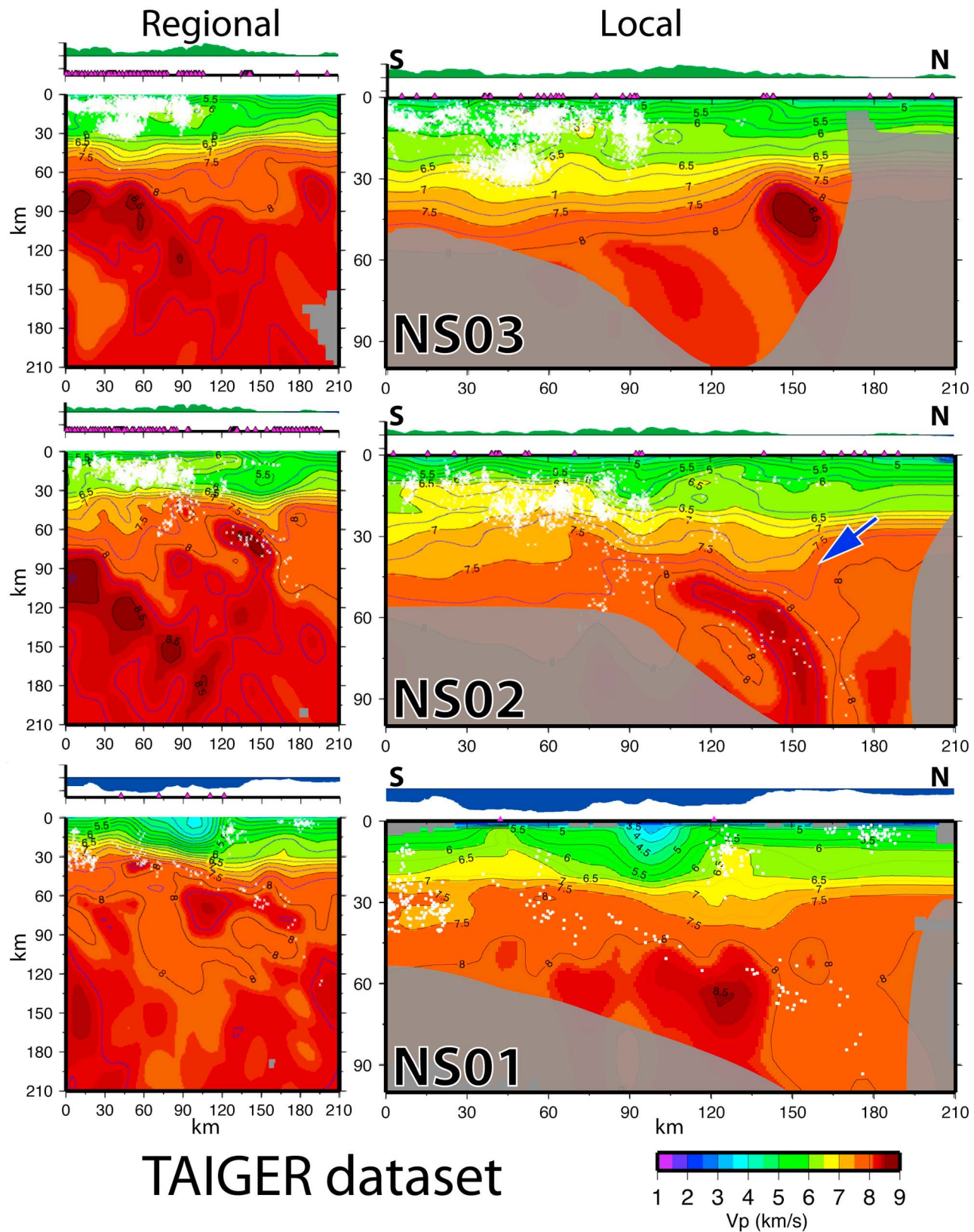


Figure 11. North-south tomographic sections of absolute velocity models. The locations of the sections are shown in Figure 1. (left) From the regional model (pf3D_{regional}). (right) From the local model (pf3D_{local}). White dots: earthquakes.

contours form an arch under the Central Range and generally the 5.5–6.5 km/sec materials are thicker than the corresponding layers to the west. Similarly, the thickness of the layer bounded by the 6–7 km/sec contours essentially doubles under the high range. Except in N02 and N03 (Figure 10) the overall trends are the same in the other sections. The overall shape of the crust preserves an east-west asymmetry; the 7.5 km/sec contour, for example, is much steeper on the east side than it is on the west.

[20] The “regional” east-west sections in the left panels of Figures 8–10 show clearly the spatial variations of the high velocity zone in the upper mantle beneath Taiwan. In S01, the high velocity zone dips east at about 62° . A similar zone can be seen in S02 and S03 but at somewhat steeper angle. In C01 it again dips at about 62° , but it becomes much steeper in C02 and then nearly vertical and more diffused in C03, N01, N02 and N03. We note that in S01 the top of the dipping high velocity zone coincides with the seismicity, indicating that the high velocity zone is associated with an active subduction zone. However, the high velocity zones in other sections to the north are not associated with seismicity.

[21] Cross-sections parallel to the structural trends of Taiwan (NS01 and NS02 in Figure 11), both onshore and just offshore of eastern Taiwan, show a northward dipping high velocity zone coinciding with the Ryukyu seismic zone (e.g., $V_p > 8.25$ km/sec; Figure 11, profile NS02). A small yet persistent feature is the low velocity zone above the Wadati-Benioff zone in profile NS02 (blue arrow near the inverted triangular area in NS02, Figure 11) and in NS03 as well. Similarly positioned features with respect to the subduction zone have been mapped under Alaska [Eberhart-Phillips *et al.*, 2006], New Zealand [Eberhart-Phillips and Reyners, 1997], and under Kanto, Japan, where the PSP subducts under the EUR [F. T. Wu *et al.*, 2007]. The strong coupling of the subducting plate with the upper plate may have dragged the latter down with it [F. T. Wu *et al.*, 2007].

5. Evaluating the Results

[22] Key considerations in the interpretation of tomographic images are resolution and robustness. To evaluate levels of resolution, we performed three tests with two checkerboard patterns (Figures 6 and 7 and Figure S1 in Text S1 of the auxiliary material) to determine whether anomalies with dimensions between 30 and 60 km, roughly the dimensions of the main structures we desire to image in the mantle, can be resolved adequately.¹ Additionally, because resolution will generally depend on the geometry of the object being resolved, we also attempt to recover anomalies of a magnitude and spatial distribution suggested by the derived tomographic images themselves, specifically by trying to recover the final model from a 1D starting model.

[23] To evaluate the pf3d_local tomography results, we perturbed a 1D background model with $\pm 10\%$ anomalies in a checkerboard pattern, and added 0.1 s random errors to the calculated travel times (Figure S2 in Text S1 of the auxiliary material). The large deviations from the background reflect the expected level of heterogeneity in the crust. The sizes of the checkers are 20 km \times 20 km \times 10 km at shallow depths,

increasing to 20 km \times 20 km \times 20 km and 20 km \times 20 km \times 30 km at greater depths (Figure S2 in Text S1 of the auxiliary material). In general, we find that the resolution in the local tomography model is reasonable down to ~ 60 km depth in central Taiwan and ~ 90 km depth in northern Taiwan above the PSP subduction zone.

[24] For the pf3d_region model, similar checkerboard tests (smaller $\pm 5\%$ mantle-like anomalies in a checkerboard pattern, and 0.1 s random errors) show that 30 \times 30 \times 30 km³ blocks appear to be well resolved to 100 km depth, and 60 \times 60 \times 60 km³ blocks to a depth of 200 km directly beneath Taiwan (Figure S1 in Text S1 of the auxiliary material). Resolution of anomalies below 200 km depth is generally poor. As may be expected, resolution at mantle depths is a simple function of station distribution (very good near the center of the network; less adequate toward the edges); because of sparse ocean-bottom recording sites, the resolution is quite poor especially at shallow depths (0–10 km) offshore of eastern Taiwan due to inadequate raypath coverage (Figures 6c and 7a).

[25] The TAIGER networks covers a relative short period of time in comparison to the TAISN and therefore far fewer earthquake sources were recorded. Although the TAIGER data set remains the best data for regional tomography, in the local model some structures in regions of relatively low seismicity, such as southern Taiwan, may not be illuminated adequately. Augmenting the TAIGER data with a subset of the TAISN data could be effective in enhancing the resolution of some structures. At present, the potential timing issues [Chou *et al.*, 2009; Chang *et al.*, 2012] prevent us from doing so. In Figure 12, our inversion results using the TAISN phase picks of Y.-M. Wu *et al.* [2007] are juxtaposed against those of using the TAIGER picks. The green shades in the checkerboard-test sections mark the regions where comparatively better resolution of the two results is achieved. We find that where the resolution of the tomographic results is reasonable for both sets of data, the first order features are quite compatible (Figure 12). As remarked previously TAIGER data sets resolve features better at shallow depths and in offshore areas. However, under southern Taiwan (S01, Figure 12) shows that the TAISN data contributes to better resolution at 45–60 km and at greater depths. If further testing confirms the proposed time corrections of Chang *et al.* [2012] the rich archive data and certainly the new TAISN data with local GPS-based time stamping can be employed to improve the images in southern Taiwan.

[26] In summary, the crustal thickening on the west side of the LVF is observed from this and previous studies (Figure S4 in Text S1 of the auxiliary material) [e.g., Kim *et al.*, 2005; Y.-M. Wu *et al.*, 2007]; they are most probably well resolved. With the addition of the OBS data, we can better resolve the structures in eastern Taiwan and offshore of eastern Taiwan and, for the first time, the crustal thickening east of the LVF is consistently mapped. The imaging of the upper mantle appears to be robust.

6. Discussion

6.1. The Thickening of Crust on Both Sides of the Collision Boundary

[27] It is well known that the crust of Taiwan has thickened under the Central Range, on the west side of the suture (LVF)

¹Auxiliary materials are available in the HTML. doi:10.1029/2011JB009108.

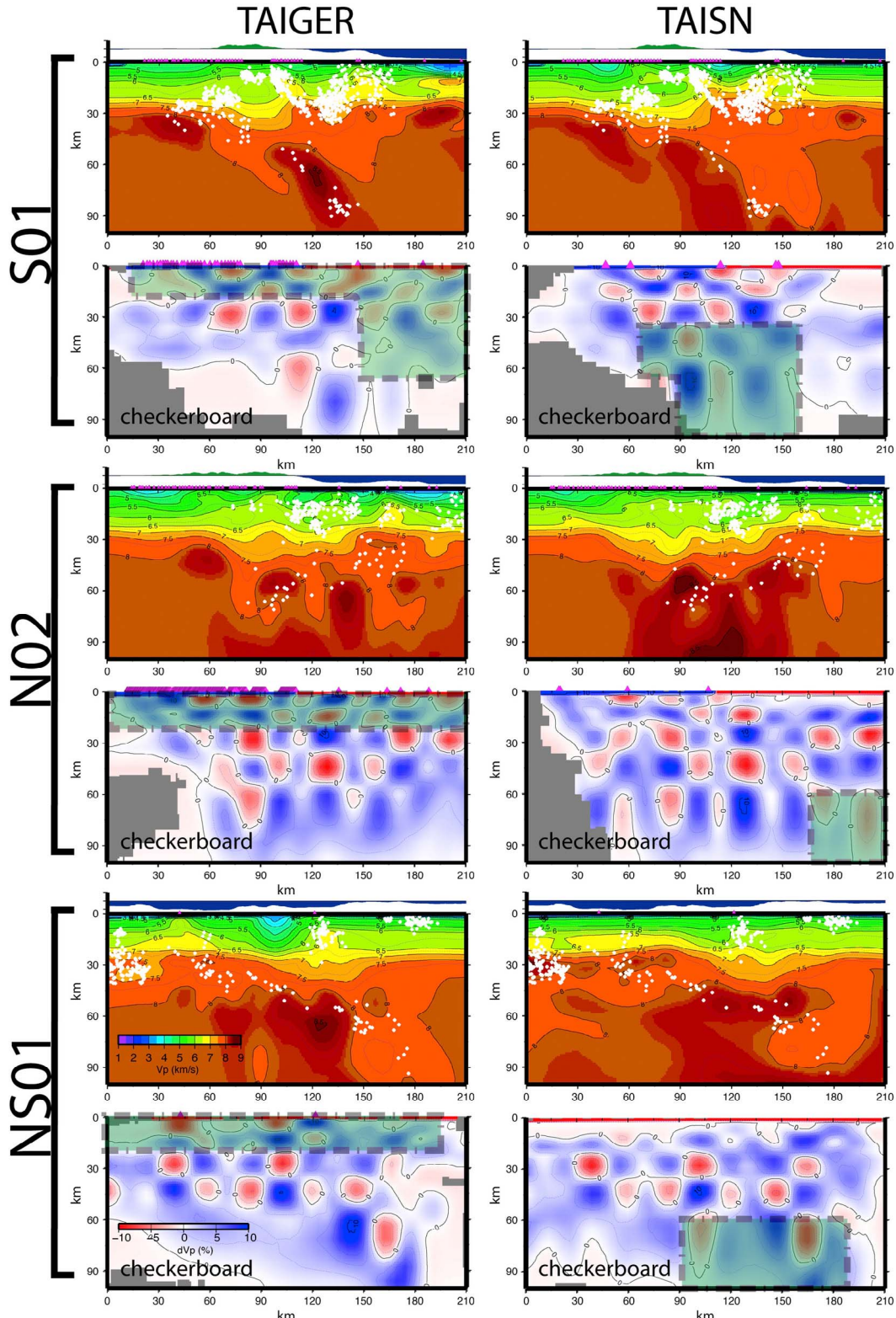


Figure 12. Comparisons of the local tomographic results from TAIGER and TAISN data sets and their associated checkerboard tests. The locations of the sections are shown in Figure 1. (left) TAIGER data only. (right) TAISN data only. The light-green shaded areas are those where the resolution for the data set is better than the other. The overall TAIGER results have better resolution at shallow depths, because of the use of active source records from explosions, and offshore of eastern Taiwan because of the ocean bottom data. The TAISN data set, with longer recording period and therefore more earthquakes from the PSP subduction zone under northern Taiwan, image the deep structures under Taiwan better.

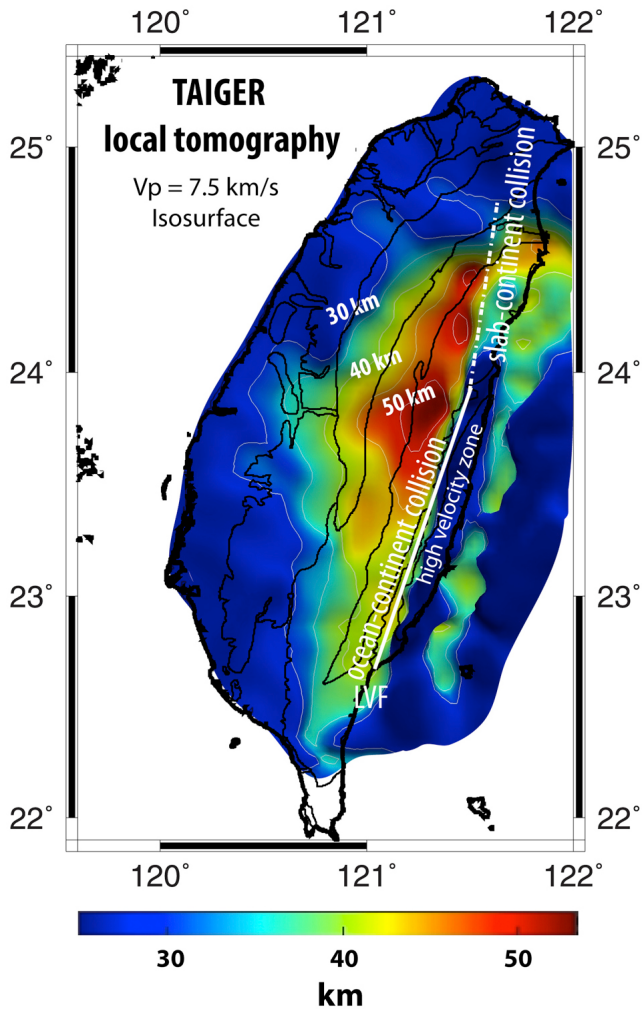


Figure 13. The depths of the 7.5 km/sec iso-surface from the local tomographic model pf3D_local. The presence of the high velocity rise between the “root” on the EUR side and the smaller “root” on the PSP side. Note also the asymmetry of the EUR root – the eastern side is much steeper than the western side.

[Rau and Wu, 1995]. As shown in Figures 8–10 and 13, the thickening is quite asymmetric, increasing gradually eastward on the west side and then decreasing sharply toward the east on the east side and its asymmetry is more pronounced than that of the topography. Comparing the profile across Taiwan to that of the continental shelf west of Taiwan [Lester et al., 2010], a candidate for the “undeformed” crust before the collision, a near doubling of the thickness under the Central Range from less than 30 km to over 50 km can be envisaged. That is a result of cumulative shortening and deformation during the collision. Overall, the crust is thickest under the Central Range between 23.5°N and 24.5°N close to the LVF (profiles C02 to N02 in Figures 9, 10, and 13), with the maximum thickness reaching more than 50 km.

[28] East of the LVF and east of the collision-compressed Coastal Range and the forearc block to the east of Taiwan we observe a smaller root-like crustal feature (Figures 8–10 and 13). The clear definition of thickened crust corroborates

the inference that shortening due to the collision occurs on both sides of the plate boundary [Hetland and Wu, 1998; Wu et al., 1997]. The existence of this root calls into question the concept of the PSP as a “rigid indenter” [e.g., Suppe, 1981; Yui and Chu, 2000]. The thickening of the Central Range crust, the creation of the Coastal Range and its root take place when the PSP and the EUR are in collision while the PSP subducts to the north (Figure 13) [Kao and Jian, 2001; Wu et al., 2009].

[29] With regard to the high velocity rise under the LVF between the Central Range and the Coastal Range (Figure 13), it has been partially mapped before by Lin et al. [1998], Kim et al. [2006] and Liang et al. [2007]. However, with data offshore of eastern Taiwan we are able to map the whole extent of this apparently continuous feature and trace its connection down to the lower crust. The rise is found in the section of Taiwan where the collision is most intense; the rise seems to form mainly from the thickening of materials with velocities between 7.5 and 8 km/sec (Figures 8 and 9). Lin [2002] linked his observed zone to exhumation of the subducted continental crusts in the Eastern Central Range, but our images indicate that much of the rise is under the Coastal Range and not rooted in the subduction zone as Lin [2002] proposed. Liang et al. [2007] looked for Pn-arrivals along the LVF and detected the high velocity zone. They interpreted the refractor as the bottom of a 23 ± 2 km crust on top of the PSP mantle under the LVF and the Coastal Range, mostly based on Kim et al. [2005].

[30] Being close to the collision suture and to the region of maximum shortening [Hsu et al., 2009] the rise may be a direct result of convergence. The upthrust of the PSP to create the Coastal Range, with concomitant erosion, consumes the top part of the PSP. In that case, the high velocity lower crust/uppermost mantle may have risen up to fill the void. Depending on when the rise was formed it could also be driven by subduction and other associated processes. Both the smaller root discussed previously and the high velocity rise are found where the forearc block, which is prominently present to the south [Malavieille et al., 2002], existed; the block may have been severely deformed in the collision to form these structures. Thus, the formation of the two roots and the high velocity rise are all parts of the collision orogen, straddling the two plates. The relative amount of deformation of the two plates implied by the sizes of these roots can be interpreted in terms of rheology, among other relevant geodynamic parameters that control the geodynamic processes. If the PSP is very strong, it may behave like a rigid plate – it can indent the continent or initiate a west-dipping subduction; if it is very weak, it may be deformed and become the more dominant topographic feature of the collision belt.

[31] The crustal features we image are detailed enough that the long-term effect of some proposed major tectonic structures, such as a through going detachment across Taiwan [e.g., Suppe, 1981; Carena et al., 2002], should be observable. A low-angle thrust fault that has been active for even one million years would result in a total displacement of about 80 km. Then the upper part of the high velocity Central Range core should be offset from its “root” by 80 km or so to the west, thus overlying the young Tertiary sediments. However, we fail to find any such offset in our model (Figures 8 and 9).

6.2. The Slab of the Eurasian Plate

[32] Our “regional” results in Figures 8 to 10 show high velocity anomalies in the upper mantle under much of Taiwan. In southern Taiwan, a Wadati-Benioff seismic zone coincides with the top of this anomaly (Figure 8, profile S01), implying active subduction under southern Taiwan. The high velocity zone continues northward, but north of about 22.8°N there is no upper mantle seismicity associated with it (Figures 8 to 10) [see also Wu *et al.*, 1997]. Its continuity with the southern, active subduction implies that this was a part of the subduction system. It may have ceased to be active, because of the buoyancy of the EUR or be involved in a seismically quiescent descent into the mantle, similar to what has been proposed for South Island, New Zealand [Molnar *et al.*, 1999] or as a result of crustal eclogitization discussed later. We observe that the magnitude of δV_p decreases and the dip of the anomaly increases toward the north and the high velocity anomalies becomes quite diffused under northern Taiwan. The diffused zone is located directly under the thickened crust of northern Taiwan and to the west of the PSP subduction zone [Wu *et al.*, 2009]; the continuous westward advance of the PSP against the EUR can conceivably lead to the destruction of organized structures in the upper mantle.

[33] Two different hypotheses have been proposed regarding the structures and processes in the upper mantle under Taiwan. Teng *et al.* [2000] suggested a southward propagating break-off of the east-dipping EUR slab with a subsequent switch to the northward subduction of the Ryukyu zone – a process called “flipping.” In this hypothesis, the switch takes place presently in northern Taiwan along a NWW line, defining the western edge of the subducting PSP, and northeast to this line the collision has started to collapse. In Teng *et al.* [2000], the hypothesized current geometry of the subduction flipping is clearly specified, with the boundary under northern Taiwan. The high velocity anomaly can be identified as an east-dipping zone starting around 23.5°N, south of the predicted location. The series of regional images for northern Taiwan (Figure 10) do not immediately suggest the breaking of the EUR and the rise of lower velocity asthenosphere as depicted in Teng *et al.* [2000, Figures 2d and 2e].

[34] Lallemand *et al.* [2001] proposed a model that includes the evolution of southwestern Ryukyu and the formation of Taiwan. The continuous tearing of the EUR by the PSP slab leads to its progressive detachment under Taiwan. It accounts for the lack of the upper mantle seismicity north of ~23°N. A series of sections (XX', YY', and ZZ' in Figure 8) in their paper depict the current plate configurations that the proposed model implies and they provide a basis for comparison with our results. We show in Figure 14 the corresponding sections from our velocity model. In XX' the subducting lithosphere can be delineated quite clearly with the aid of the high velocity anomaly and the seismicity; the PSP appears to terminate below the continental crust. The curve that defines the EUR high velocity anomaly is also clear. The YY' and ZZ' sections can be interpreted similarly. The central question is whether an insertion of the PSP into the EUR indicated in Lallemand *et al.* [2001] has occurred. It is tempting to conclude from the dV_p images in Figure 14 as evidence for the insertion of the PSP. However, there is a lack of clear V_p

signatures in the same figure that can be interpreted as the PSP between the EUR. Much follow-up work will aim toward refinement in interpretation. In both models [Teng *et al.*, 2000; Lallemand *et al.*, 2001], one would assume that the flipping or breaking an actively subducting slab is a mechanically violent process and the seismicity associated with the processes would be high, a condition not found in the upper mantle under Taiwan.

[35] We note that the “root” under the Central Range, as defined by the 7.5 km/sec contour, ranges from about 40 km (Figure 8, S01-S03) to about 50 km, generally lies directly on top of the high velocity anomaly. Rocks deeper than about 40 km in a continental mountain root can be completely converted to eclogite, with an accompanying increase in density [Ryan, 2001], especially in the presence of water [Leech, 2001]. The P velocities in the upper mantle between 60 and 160 km below Taiwan are as high as 8.5 km/sec in the south and range from 8.1 to 8.2 km/sec in the north, (Figure 8, S01-S03, Figure 9, C01-C02) and the higher velocity zones could perhaps be a consequence of eclogitization [Christensen and Mooney, 1995]. Consistent with the tectonics of Taiwan, these materials could result from metamorphism of either basic oceanic rocks belonging to the Eurasian plate or from the lower continental crust [Leech, 2001]. The former implies that a piece of mafic oceanic lithosphere has been subducted and eclogitization has taken place. The latter process is more complex. Leech [2001] proposes that a good amount of water is required for the eclogitization of continental crust to proceed, but, once it is formed, then the negative buoyancy of eclogite with respect to the surrounding rocks may lead to its descent through the crust-mantle boundary. There are two mechanisms to provide water in the lower crust: one is from a dehydration process of metamorphic belts and the other is from fluid infiltrating the fractures induced by local earthquakes as summarized by Wittlinger *et al.* [2009]. Both of the processes are possible for the Taiwan orogen, because the metamorphic belts are just above the high velocity zone in the upper mantle as well as the earthquakes occurred frequently in the lower crust on the both side of a thickened crust (Figure 9). Upon eclogitization the high density materials would lead to foundering and possibly delamination; Ryan [2001] conjectured that in an active orogen it could be an ongoing process. Our cross sections show a thickened crust overlying the high velocity zone without an interposing low velocity zone, implying that if delamination has taken place the asthenospheric rise has not yet occurred.

7. Conclusions

[36] New tomographic V_p models of the crust and upper mantle down to about 200 km beneath Taiwan have been derived from the TAIGER seismic deployments and permanent broadband stations on Taiwan. The “local” model is based on the arrival times of seismic waves from land explosions and earthquakes in and around Taiwan and the “regional” model incorporates additional picks from teleseisms. Although some of the major crustal features imaged in our local model are similar to those of Rau and Wu [1995] and Kim *et al.* [2005], thus demonstrating their robustness, several significant, new crustal and mantle velocity structures were imaged as a result of the increased aperture of the

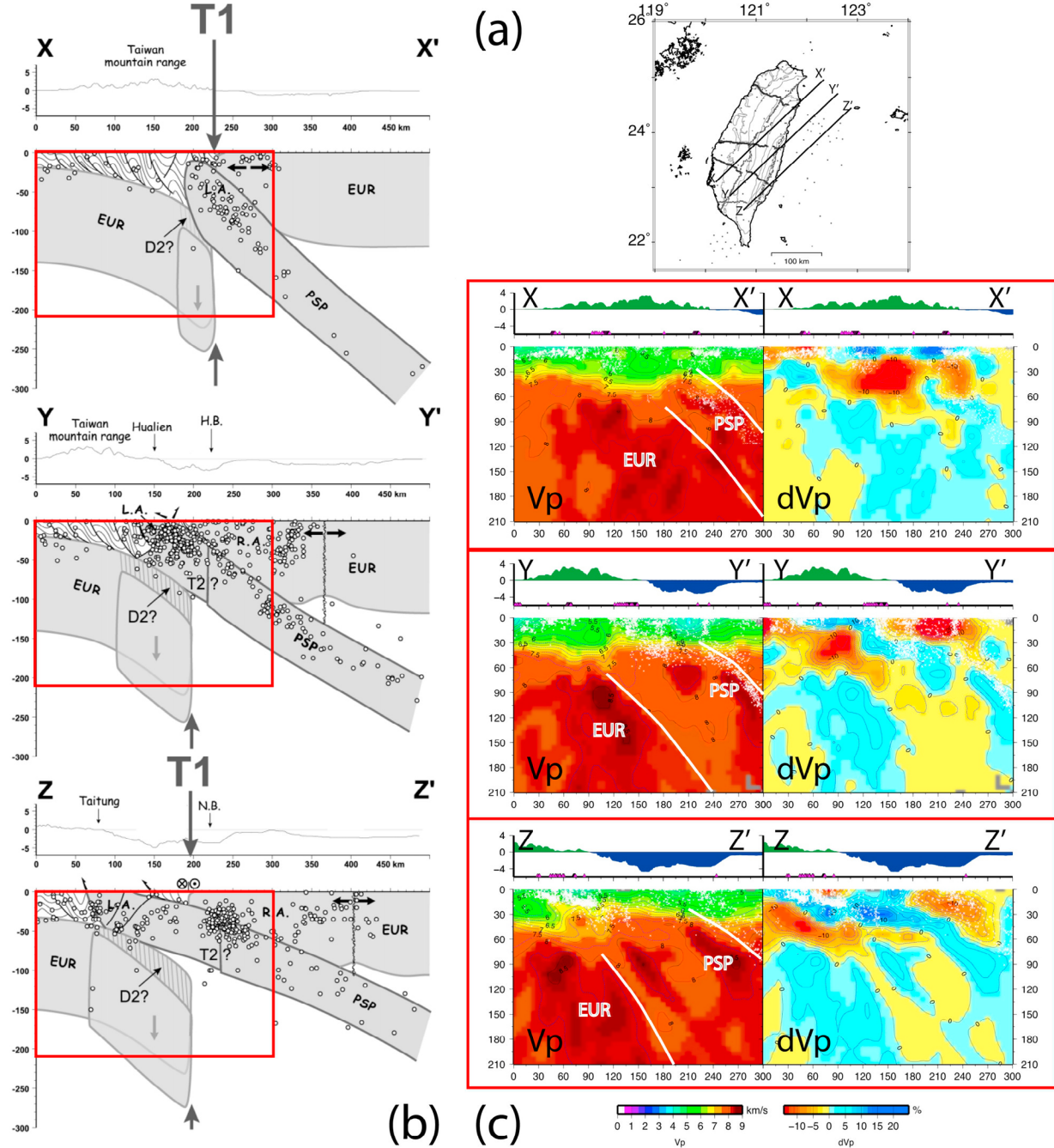


Figure 14. Tomographic sections along three profiles from *Lallemand et al. [2001]* and plate tectonic interpretations. (a) Locations of the interpreted seismological sections from *Lallemand et al. [2001]* and the tomographic sections. (b) Three SW-NE interpreted seismological sections from *Lallemand et al. [2001]*. T1: tear fault; D2: slab detachment; L.A.: Luzon Arc; R.A.: Ryukyu Arc. Symbol-white circle: earthquake. Red rectangle: region of the interpreted cross-section corresponding to that of the tomographic section in Figure 14c. (c) XX' tomographic cross-section: the seismicity and the high velocity anomalies are used here to define the PSP subduction zone and the EUR high velocity zone under Taiwan. The PSP crust does not extend into the crust as predicted in the model in Figure 14b. YY' tomographic cross-section: the PSP and the EUR are defined the same manner as in the XX' cross-section. Under the EUR, the crustal depth increases sharply as shown in Figure 8 and 9. The section slices diagonally to the strike of the Ryukyu subduction zone. ZZ' tomographic cross-section: the PSP and the EUR are defined as in the XX' and YY' cross-sections. In this section, the high velocity rise and the eastern root appear. Notice the dipping seismic zone seen in the shallow part of the section on the left is the ChengKung seismic zone and it is part of the island parallel thrust structures that created the Coastal Range, and therefore it is not related to the northward moving PSP. White dot: earthquake. White line: plate boundary.

station network and the inclusion of teleseismic data. The more complete and better resolved images of the high velocity rise under the LVF/Coastal Range and the thickened EUR and PSP point toward a broad zone of orogenic deformation that need to be taken into account in geodynamic modeling of Taiwan. The upper mantle high velocity anomaly along the trend of Taiwan can be identified as a seismically active subduction zone in southern Taiwan, and a seismically quiescent zone under south central Taiwan. The anomaly under south central Taiwan zone shows that subduction of the EUR was occurring, at least, in the not too distant, geologic past. The lack of associated seismicity with the anomaly in central Taiwan and the disappearance of the organized high velocity anomalies under northern Taiwan suggest the stoppage of eastward subduction toward the north. With the crust on the EUR side thickened to more than 50 km, the possibility of complex petrological changes in the lower crust, including eclogitization, could lead to the transfer of crustal material into the high velocity zone.

[37] Although the spatial resolution of our tomography is not comparable to those of the geologic maps of Taiwan, the images provide critical structural information in the third dimension. The use of the new Vp model in reviewing the existing tectonic models and in investigating the geodynamics of the Taiwan orogeny is a fertile field. On the basis of the present work, research using TAIGER data is being carried out in the determination of Vp/Vs ratios, providing more constraints for crustal composition.

[38] **Acknowledgments.** A major project such as TAIGER involves the intense effort of many collaborative scientists. This paper is among the earlier products of this project and this research is possible only with the long and arduous efforts of D. Okaya (USC) and C.-Y. Wang (NCU, Taiwan) for active source experiments; B.-S. Huang (IES, Taiwan) for passive deployments; K. McIntosh (UTIG), Y. Nakamura (UTIG), C.-S. Lee (NTOU, Taiwan), and C.-S. Liu (NTU, Taiwan) for marine MCS and OBS deployment and retrieval; as well as W.-T. Liang (IES, Taiwan) for helping data archiving. L. Lavie's (UTIG) guidance in geodynamics helped us with the big pictures. The crews of R/V *Langseth* (Lamont Geological Observatory) and many supporting Taiwanese vessels and the staff of the Ocean Bottom Seismometer Instrument Pool (OBSIP) provided efficient and reliable services. Finally, we acknowledge the financial support (EAR0410227 and EAR1010645) of Continental Dynamics Program (EAR) and logistic support of the Integrative Programs (OCE) of National Science Foundation. IRIS/PASSCAL and OBSIP provided land and ocean bottom instrumentation, respectively. The National Science Council in Taiwan funded our Taiwanese colleagues. This work was also supported by a PhD scholarship from the Ministry of Education of Taiwan to H.K.-C.

References

- Bijwaard, H., W. Spakman, and E. R. Engdahl (1998), Closing the gap between regional and global travel time tomography, *J. Geophys. Res.*, **103**, 30,055–30,078, doi:10.1029/98JB02467.
- Biq, C. (1981), Collision. Taiwan-style, *Mem. Geol. Soc. China*, **4**, 91–102.
- Bos, A. G., W. Spakman, and M. C. J. Nyst (2003), Surface deformation and tectonic setting of Taiwan inferred from a GPS velocity field, *J. Geophys. Res.*, **108**(B10), 2458, doi:10.1029/2002JB002336.
- Carena, S., J. Suppe, and H. Kao (2002), Active detachment of Taiwan illuminated by small earthquakes and its control of first-order topography, *Geology*, **30**, 935–938, doi:10.1130/0091-7613(2002)030<0935:ADOTIB>2.0.CO;2.
- Chai, B. H. T. (1972), Structure and tectonic evolution of Taiwan, *Am. J. Sci.*, **272**, 389–422, doi:10.2475/ajs.272.5.389.
- Chang, C. H., Y. M. Wu, D. Y. Chen, T. C. Shin, T. L. Chin, and W. Y. Chang (2012), An examination of telemetry delay in the Central Weather Bureau seismic network, *Terr. Atmos. Oceanic Sci.*, doi:10.3319/TAO.2011.11.29.01(T), in press.
- Chen, C. H., Y. H. Chen, H. Y. Yen, and G. K. Yu (2003), Lateral variations of Pn velocity and anisotropy in Taiwan from travel-time tomography, *Earth Planets Space*, **55**, 223–230.
- Chou, H.-C., B.-Y. Kuo, L.-Y. Chiao, D. Zhao, and S.-H. Hung (2009), Tomography of the westernmost Ryukyu subduction zone and the serpentinization of the fore-arc mantle, *J. Geophys. Res.*, **114**, B12301, doi:10.1029/2008JB006192.
- Christensen, N. I., and W. D. Mooney (1995), Seismic velocity structure and composition of the continental crust: A global view, *J. Geophys. Res.*, **100**(9), 9761–9788.
- Eberhart-Phillips, D., and M. Reyners (1997), Continental subduction and three-dimensional crustal structure: The northern South Island, New Zealand, *J. Geophys. Res.*, **102**(B6), 11,843–11,861, doi:10.1029/96JB03555.
- Eberhart-Phillips, D., D. H. Christensen, T. M. Brocher, R. Hansen, N. A. Ruppert, P. J. Haeussler, and G. A. Abers (2006), Imaging the transition from Aleutian subduction to Yakutat collision in central Alaska, with local earthquakes and active source data, *J. Geophys. Res.*, **111**, B11303, doi:10.1029/2005JB004240.
- Hetland, E. A., and F. T. Wu (1998), Deformation of the Philippine Sea Plate under the Coastal Range, Taiwan: Results from an offshore-onshore seismic experiment, *Terr. Atmos. Oceanic Sci.*, **9**, 363–378.
- Ho, C. S. (1986), *An Introduction to the Geology of Taiwan: Explanatory Text of the Geologic Map of Taiwan*, Cent. Geol. Surv., Taiwan.
- Hole, J. A., and B. C. Zelt (1995), 3-D finite-difference reflection traveltimes, *Geophys. J. Int.*, **121**, 2427–2434.
- Hsu, Y., S. Yu, M. Simons, L. Kuo, and H. Chen (2009), Interseismic crustal deformation in the Taiwan plate boundary zone revealed by GPS observations, seismicity, and earthquake focal mechanisms, *Tectonophysics*, **479**, 4–18, doi:10.1016/j.tecto.2008.11.016.
- Kao, H., and P.-R. Jian (2001), Seismogenic patterns in the Taiwan region: Insights from source parameter inversion of BATS data, *Tectonophysics*, **333**, 179–198, doi:10.1016/S0040-1951(00)00274-2.
- Kim, K. H., J. M. Chiu, J. Pujol, K. C. Chen, B. S. Huang, Y. H. Yeh, and P. Shen (2005), Three-dimensional VP and VS structural model associated with the active subduction and collision tectonics in the Taiwan region, *Geophys. J. Int.*, **162**, 204–220, doi:10.1111/j.1365-246X.2005.02657.x.
- Kim, K. H., J. M. Chiu, J. Pujol, and K. C. Chen (2006), Polarity reversal of active plate boundary and elevated oceanic upper mantle beneath the collision suture in central eastern Taiwan, *Bull. Seismol. Soc. Am.*, **96**, 796–806.
- Kuo-chen, H., Y. M. Wu, Y. G. Chen, and R. Y. Chen (2007), 2003 Mw6.8 Chengkung earthquake and its associated seismogenic structures, *J. Asian Earth Sci.*, **31**, 332–339, doi:10.1016/j.jseas.2006.07.028.
- Lallemand, S., Y. Font, H. Bijwaard, and H. Kao (2001), New insights on 3-D plates interaction near Taiwan from tomography and tectonic implications, *Tectonophysics*, **335**, 229–253, doi:10.1016/S0040-1951(01)00071-3.
- Leech, M. L. (2001), Arrested orogenic development: Eclogitization, delamination, and tectonic collapse, *Earth Planet. Sci. Lett.*, **185**, 149–159, doi:10.1016/S0012-821X(00)00374-5.
- Lester, W. R., K. McIntosh, and H. van Avendonk (2010), Crustal-scale structure of the Eurasian Continental Margin in the northern South China Sea, offshore Taiwan from seismic reflection data, *Eos Trans. AGU*, **91**(26), West. Pac. Geophys. Meet. Suppl., Abstract T21A-071.
- Liang, W.-T., J.-M. Chiu, and K. Kim (2007), Anomalous Pn waves observed in Eastern Taiwan: Implications of a thin crust and elevated oceanic upper mantle beneath the active collision-zone suture, *Bull. Seismol. Soc. Am.*, **97**, 1370–1377.
- Liao, Y. C., S.-K. Hsu, C.-H. Chang, W.-B. Doo, M.-Y. Ho, C.-L. Lo, and C.-S. Lee (2008), Seismic tomography off SW Taiwan: A joint inversion from OBS and onshore data of 2006 Pingtung aftershocks, *Terr. Atmos. Oceanic Sci.*, **19**, 729–741, doi:10.3319/TAO.2008.19.6.729(PT).
- Lin, A. T., and A. B. Watts (2002), Origin of the West Taiwan Basin by orogenic loading and flexure of a rifted continental margin, *J. Geophys. Res.*, **107**(B9), 2185, doi:10.1029/2001JB000669.
- Lin, C. H. (2002), Active continental subduction and crustal exhumation: The Taiwan orogeny, *Terra Nova*, **14**, 281–287, doi:10.1046/j.1365-3121.2002.00421.x.
- Lin, C. H., Y. H. Yeh, H. Y. Yen, K.-C. Chen, B.-S. Huang, S. W. Roecker, and J.-M. Chiu (1998), Three-dimensional elastic velocity structure of the Hualien region of Taiwan—evidence of active crustal exhumation, *Tectonics*, **17**, 89–103, doi:10.1029/97TC02510.
- Ma, K. F., and D. R. Song (1997), Pn velocity and Moho depth in Taiwan, *J. Geol. Soc. China*, **40**, 167–184.
- Ma, K. F., J. H. Wang, and D. Zhao (1996), Three-dimensional seismic velocity structure of the crust and uppermost mantle beneath Taiwan, *J. Phys. Earth*, **44**, 85–105, doi:10.4294/jpe1952.44.85.
- Maeda, N. (1985), A method for reading and checking phase times in auto-processing system of seismic wave data, *J. Seismol. Soc. Jpn.*, **38**, 365–379.

- Malavieille, J., S. E. Lallemand, S. Dominguez, A. Deschamps, C.-Y. Lu, C.-S. Liu, P. Schmurl, and A. S. Crew (2002), Arc-continent collision in Taiwan: New marine observations and tectonic evolution, *Spec. Pap. Geol. Soc. Am.*, 358, 189–213.
- McIntosh, K., Y. Nakamura, T. K. Wang, R. C. Shih, A. Chen, and C. S. Liu (2005), Crustal-scale seismic profiles across Taiwan and the western Philippine Sea, *Tectonophysics*, 401, 23–54, doi:10.1016/j.tecto.2005.02.015.
- Molnar, P., et al. (1999), Continuous deformation versus faulting through the continental lithosphere of New Zealand, *Science*, 286, 516–519, doi:10.1126/science.286.5439.516.
- Rau, R. J., and F. T. Wu (1995), Tomographic imaging of lithospheric structures under Taiwan, *Earth Planet. Sci. Lett.*, 133, 517–532, doi:10.1016/0012-821X(95)00076-O.
- Roecker, S. W., Y. H. Yeh, and Y. B. Tsai (1987), Three-dimensional P and S wave velocity structures beneath Taiwan—deep structure beneath an arc-continent collision, *J. Geophys. Res.*, 92, 10,547–10,570.
- Roecker, S., C. Thurber, and D. McPhee (2004), Joint inversion of gravity and arrival time data from Parkfield: New constraints on structure and hypocenter locations near the SAFOD drill site, *Geophys. Res. Lett.*, 31, L12S04, doi:10.1029/2003GL019396.
- Roecker, S., C. Thurber, and K. Roberts (2006), Refining the image of the San Andreas Fault near Parkfield, California using a finite difference travel time computation technique, *Tectonophysics*, 426, 189–205, doi:10.1016/j.tecto.2006.02.026.
- Ryan, P. D. (2001), The role of deep basement during continent-continent collision: A review, in *Continental Reactivation and Reworking*, edited by J. A. Miller et al., *Geol. Soc. Spec. Publ.*, 184, 39–55, doi:10.1144/GSL.SP.2001.184.01.03.
- Shin, T. C., and Y. L. Chen (1988), Study on the earthquake location of 3-D velocity structure in the Taiwan area, *Meteorol. Bull.*, 42, 135–169.
- Suppe, J. (1981), Mechanics of mountain-building and metamorphism in Taiwan, *Mem. Geol. Soc. China*, 4, 67–89.
- Teng, L. S., C. T. Lee, Y. B. Tsai, and L.-Y. Hsiao (2000), Slab breakoff as a mechanism for flipping of subduction polarity in Taiwan, *Geology*, 28, 155–158, doi:10.1130/0091-7613(2000)28<155:SBAAMF>2.0.CO;2.
- Theunissen, T., S. Lallamand, Y. Font, S. Gautier, C.-S. Lee, W.-T. Liang, F.-T. Wu, and T. Berthet (2012), Crustal deformation at the southernmost part of the Ryukyu Subduction (East Taiwan) as revealed by new marine seismic experiments, *Tectonophysics*, doi:10.1016/j.tecto.2012.04.011, in press.
- Vidale, J. E. (1988), Finite-difference calculation of travel times, *Bull. Seismol. Soc. Am.*, 78, 2062–2076.
- Wang, Z., D. Zhao, J. Wang, and H. Kao (2006), Tomographic evidence for the Eurasian lithosphere subducting beneath south Taiwan, *Geophys. Res. Lett.*, 33, L18306, doi:10.1029/2006GL027166.
- Wang, Z., Y. Fukao, D. Zhao, S. Kodaira, O. P. Mishra, and A. Yamada (2009), Structural heterogeneities in the crust and upper mantle beneath Taiwan, *Tectonophysics*, 476, 460–477, doi:10.1016/j.tecto.2009.07.018.
- Wittlinger, G., V. Farra, G. Hetényi, J. Vergne, and J. Nábělek (2009), Seismic velocities in Southern Tibet lower crust: A receiver function approach for eclogite detection, *Geophys. J. Int.*, 177, 1037–1049.
- Wu, F. T., R. J. Rau, and D. Salzberg (1997), Taiwan orogeny: Thin-skinned or lithospheric collision?, *Tectonophysics*, 274, 191–220, doi:10.1016/S0040-1951(96)00304-6.
- Wu, F. T., D. Okaya, H. Sato, and N. Hirata (2007), Interaction between two subducting plates under Tokyo and its possible effects on seismic hazards, *Geophys. Res. Lett.*, 34, L18301, doi:10.1029/2007GL030763.
- Wu, F. T., W.-T. Liang, J.-C. Lee, H. Benz, and A. Villaseñor (2009), A model for the termination of the Ryukyu subduction zone against Taiwan: A junction of collision, subduction/separation, and subduction boundaries, *J. Geophys. Res.*, 114, B07404, doi:10.1029/2008JB005950.
- Wu, Y.-M., C.-H. Chang, L. Zhao, J. B. H. Shyu, Y.-G. Chen, K. Sieh, and J.-P. Avouac (2007), Seismic tomography of Taiwan: Improved constraints from a dense network of strong-motion stations, *J. Geophys. Res.*, 112, B08312, doi:10.1029/2007JB004983.
- Yu, S. B., H. Y. Chen, and L. C. Kuo (1997), Velocity of GPS stations in the Taiwan area, *Tectonophysics*, 274, 41–59, doi:10.1016/S0040-1951(96)00297-1.
- Yui, T. F., and H. T. Chu (2000), “Overturned” marble layers: Evidence for upward extrusion of the Backbone Range of Taiwan, *Earth Planet. Sci. Lett.*, 179, 351–361, doi:10.1016/S0012-821X(00)00119-9.